Acta Crystallographica Section A
**Foundations of Crystallography**
ISSN 0108-7673

Received 21 January 2007
Accepted 12 March 2007



# Kinematical multiple diffraction: the width of $\psi$-scan intensity profiles

**Elisabeth Rossmanith**

Mineralogisch-Petrographisches Institut der Universität Hamburg, D-20146 Hamburg, Grindelallee 48, Germany. Correspondence e-mail: rossmanith@mineralogie.uni-hamburg.de

It was shown in Rossmanith [*Acta Cryst.* (1992), A**48**, 596–610] that the peak width of intensity profiles of multiple diffraction events can be calculated in a simple manner from the divergence $\delta$ and the wavelength spread $\Delta\lambda/\lambda$ of the incident beam and from the mosaic spread $\eta$ and the magnitude $r$ of the ideally perfect crystallites in the sample. In the present paper, an improvement of the concept is given.

## 1. Introduction

The perturbation of the intensity of any primary reflection caused by multiple diffraction can be handled *exactly* only in the framework of the dynamical theory (Renninger, 1937, §7), *i.e.* the infinite system of fundamental equations [see for example von Laue, 1960, expression (26.32)] has to be solved. According to Renninger (1937), '... such a solution is missing until now. But even if such a solution could be found, ..., it would be applicable only for the ideally perfect crystal and would strongly depend on the shape of the sample in consideration.'

Up to now, several authors have proposed approaches to the problem. All these approaches have two requirements in common. First of all, the solutions are limited to semi-infinite plane-parallel perfect crystal slabs. Secondly, the number of equations is reduced to $N$ equations, where $N$ is the number of reciprocal-lattice points lying simultaneously very close to or on the Ewald sphere [see for example von Laue's expression (27.5) for the two-beam case and expressions (27.15) for the three-beam case]. Anyway, the absence of the *Aufhellung* terms in the result, equation (27.16), given by von Laue for a very special three-beam case, indicates that reducing the infinite system of fundamental equations to a system of three equations results in an improper solution, *i.e.* at least more than three equations have to be used. Unfortunately, the system of fundamental equations with more than two equations is not solvable exactly. Numerical methods are proposed by several authors instead. Nevertheless, until now, in the framework of the dynamical theory, 'theoretical fitting of the profiles is only possible in exceptional cases where the diffraction geometry is accurately known' (Weckert & Hümmer, 1997, page 133, right column).

According to Renninger, therefore, '... it can be expected that in practice ... more primitive considerations may render the same service as an exact theory, whose requirements are poorly fulfilled.' Consequently, in chapter 7 of his famous paper, Renninger discussed two kinematical approaches, the 'simplest approach' (*einfachster Ansatz*) and a 'more sophisticated approach' (*verfeinerter Ansatz*), which is similar to the approximate kinematical approach presented by Moon & Shull (1964), who considered multiple diffraction in imperfect crystals as an extension of the theory of secondary extinction by generalizing the power-transfer equations of two-beam cases. Interference effects as well as multiple diffraction (primary extinction) inside the coherent blocks of the mosaic crystal were neglected.

The author's concept (Ro-06-§2),[1] on the other hand, is based on Renninger's 'simplest approach' for the evaluation of the integrated intensities [Ro-00-(§2.1)], combined with the results of classical optics [Ro-04-(6)] and the derivation of the phase of the complex interference function in the framework of the kinematical theory [Ro-04-(Appendix A)]. Furthermore, for the evaluation of the distribution of the integrated intensity during $\psi$ scans, the knowledge of the profile width and Lorentz factors is essential. Because of considerable shortcomings of previous expressions given in the literature for the Lorentz factor (Moon & Shull, 1964; Prager, 1971; Chang & Post, 1975; Unangst & Melle, 1975; Post, 1975, 1976) and the peak width (Collela & Merlini, 1966; Caticha-Ellis, 1975; Cousins *et al.*, 1978), a new concept for the evaluation of the Lorentz factors and peak widths derived by means of purely geometrical considerations in reciprocal space was developed (Ro-92). Based on this concept, the program *UMWEG-90* was written. Satisfactory agreement between calculated $\psi$ scans and those measured by the author's team could be obtained in all cases of forbidden primary reflections (Bengel, 1991; Werner, 1993; Rossmanith *et al.*, 1994; Rossmanith & Bengel, 1995), with one exception, the pattern of the 882 primary reflection of YIG. The concept was therefore reanalysed in 1995. Because of Mathieson's (1994) rejection of

[1] Most of the expressions and figures discussed in this paper were derived or presented in previous papers of the author. These expressions, figures, Appendices *etc.* will be referenced in the following by the abbreviation Ro-*xxy*-(*z*), where *xx* represents the last two digits of the year of publication, *y* stands for *a*, *b*, *c etc.* if more than one paper in the respective year is referenced, and *z* represents the number of the expression, figure, Appendix *etc.* under consideration.

the author's concept for the evaluation of the width of reflection peaks, it was not possible to publish the modification before a thorough analysis of the shape and width of intensity profiles, which was finally presented in Ro-02*a* and Ro-02*b*. In §2, the modified derivation of the profile widths of multiple diffraction events will be discussed. In §3, two application examples will be presented, one for pure *Umweganregung* (the forbidden 882 primary reflection of YIG) and one for multiple diffraction (the very strong $\bar{1}\bar{1}1$ primary reflection of Si).

## 2. Modified derivation of the profile width of multiple diffraction events

Starting with Ro-00-(1) given by Renninger (1937), it was shown in Ro-00-(§2) and Ro-00-(§3.1) that the power received in the counter during the rotation about the $\psi$ axis is given by [Ro-06-(5)]

$$I_{s_1}^{(\omega)}(\psi) = \{I_{\rm prim}^{(\omega)} - I_{Aufh}^{(\omega,\psi)} f(\psi)\} + I_{Umweg}^{(\omega,\psi)} f(\psi) + I_{\rm interfer}^{(\omega)}(\psi), \quad (1)$$

where $I_{\rm prim}^{(\omega)}$ is the intensity of the primary reflection integrated with respect to the $\omega$ rotation, $I_{Aufh}^{(\omega,\psi)}$ and $I_{Umweg}^{(\omega,\psi)}$ are the intensities of the *Aufhellung* and *Umweganregung* term, respectively, integrated with respect to both axes, $\omega$ and $\psi$ [Ro-06-(6)]. $I_{\rm interfer}^{(\omega)}(\psi)$ is the interference term defined in Ro-06-(7) and $f(\psi)$ is a normalized distribution function.

It was found by comparisons of theoretical and experimental multiple diffraction patterns that $f(\psi)$ can be well approximated by an asymmetric normalized split-pseudo-Voigt function consisting of two halves, $PV(\psi)_{\rm left}$ and $PV(\psi)_{\rm right}$, with different widths and different mixing parameters for the left and right side, respectively, but with a common maximum value, where PV($\psi$) is the normalized pseudo-Voigt function [Ro-02*b*-(Appendix *A*) and Ro-02*b*-(Fig. 14)]

$$\mathrm{PV}(\psi) = \frac{1}{\Delta\psi_{\rm integral}^{\rm total}}\left[(1-\eta_{LG})\exp\left\{-\pi\left(\frac{\psi-\psi_0}{\Delta\psi_{\rm integral}^{\rm total}}\right)^2\right\} + \eta_{LG}\frac{1}{1+\left(\frac{\pi(\psi-\psi_0)}{\Delta\psi_{\rm integral}^{\rm total}}\right)^2}\right]. \quad (2)$$

$\psi_0$ corresponds to the value of the variable in the peak maximum. The mixing parameter $\eta_{\rm LG}$ is a measure of the Lorentzian contribution to the pseudo-Voigt distribution. $\Delta\psi_{\rm integral}^{\rm total}$, the total integral width of the distribution with respect to the rotation about the $\psi$ axis, mainly depends on the radius of the perfect crystallites and the divergence and wavelength spread of the incident beam. In the case of a mosaic crystal, additionally the mosaic spread will broaden the distribution:

$$\Delta\psi_{\rm integral}^{\rm total} = (\Delta\psi_{\rm crystal\,size} + \Delta\psi_{\rm divergence} + \Delta\psi_{\rm wavelength\,spread} + \Delta\psi_{\rm mosaic\,spread}), \quad (3)$$

*i.e.* the width $\Delta\psi_{\rm integral}^{\rm total}$ is approximated by the sum of the contributions (see Ro-02*b*).

The concept of the evaluation of the distribution widths by means of purely geometrical considerations is discussed in detail in Ro-92-(§II.*A*.1) for single diffraction and in Ro-92-(§II.*B*.*b*.1) for multiple diffraction.

The reasoning concerning the peak broadening in the case of multiple diffraction is based on the considerations underlying the figures Ro-92-(Figs. 3*a*–*d*), in which the dependence of the peak width on the radius $r$ of an ideally perfect crystal sphere, the wavelength spread, $\Delta\lambda/\lambda$, the beam divergence, $\delta$, and the mosaic spread, $\eta$, are graphically represented. The knowledge of these figures and Ro-92-(§II.*A*.1) is indispensable for the understanding of Ro-92-(Figs. 8*a*, *b*), in which the elevation and section plane of the geometry in reciprocal space, given in Ro-92-(Fig. 2), with respect to the direction of the $\psi$ axis for a real experiment are shown. For reasons discussed below, Ro-92-(Figs. 8*a*, *b*) have to be replaced by Fig. 1 of the present paper.

It is obvious from Fig. 1 as well as Ro-92-(Fig. 8*a*) that, in contrast to the condition during the $\omega$ rotation (called $\theta$ rotation in Ro-92), the reciprocal-lattice point $B$ belonging to the primary reflection $\mathbf{h}_{\rm prim}$ (= $OB$ in Fig. 1) as well as to the cooperative reflection $\mathbf{h}_{\rm coop}$ (= $SB$ in Fig. 1) does not move during $\psi$ rotation, *i.e.* both reflections remain in the reflection position.

For $\omega = \theta_{\rm prim}$, where $\theta_{\rm prim}$ is the Bragg angle of the primary reflection, in the case of Ro-92-(Fig. 8*a*) the effective divergence of the beam in the plane defined by the incident ray and the vector $\mathbf{h}_{\rm prim}$ is limited by the angle $\delta_{p,\rm eff} = \text{minimum}(\delta_p, \eta)$ between the rays $a$ and $b$, where $\delta_p$ is the divergence of the incident beam in the plane of Ro-92-(Fig. 8*a*), $M$ is the centre of the Ewald sphere with radius $1/\lambda$, $M_{1a}$, $M_{1b}$ are the centres of the spheres $S1a$, $S1b$ both with the radius $1/(\lambda + \Delta\lambda/2) - \varepsilon$, and $M_{2a}$, $M_{2b}$ are the centres of the spheres $S2a$, $S2b$, both with radius $1/(\lambda - \Delta\lambda/2) + \varepsilon$, where $\varepsilon = 1/r$. The peak width $\Delta\psi$ of the multiple diffraction event during $\psi$ rotation can be deduced from Ro-92-(Fig. 8*b*) and is obviously given by Ro-92-(17) and Ro-92-(18) (the relation between the width at half maximum, FWHM, and the integral width is discussed in Ro-02*b* and will not be considered in the present paper):

$$\Delta\psi_{\rm integral}^{\rm total} = \beta_2 - \beta_1 + \delta_{s,\psi} + \eta_{\psi}^{\rm op}. \quad (4)$$

Unlike Fig. 1 of the present paper, Fig. 8(*a*) in Ro-92, defining the profile width of the multiple diffraction events, is not symmetrical with respect to the section plane passing through the centre $M$ normal to the $\psi$ axis, *i.e.* it is not symmetrical with respect to the plane 0 defined in Fig. 1. Consequently, a larger width is expected for an operative reflection whose reciprocal-lattice point [$O'$ in Ro-92-(Fig. 8*a*)] passes the Ewald sphere above plane 0 (for example plane 1 defined in Fig. 1) than for an event passing the Ewald sphere below plane 0 having the same distance from plane 0 (plane 2 defined in Fig. 1). This asymmetry results from the assumption made in 1992 that, for each ray between the rays $a$ and $b$, all wavelengths in the range $\lambda - \Delta\lambda/\lambda \leq \lambda \leq \lambda + \Delta\lambda/\lambda$ contribute to

the diffraction process. As will be shown in §3, no experimental evidence could be found for this assumption.

The concept introduced in 1992 was therefore reanalysed in 1995 to take into account the experimental result obtained for the 882 primary reflection of YIG (Fig. 3*b*) as well as the reasoning corresponding to Ro-93-(Fig. 2) (see the text on the lower half right column on page 82 in Ro-93): *i.e.* if only those wavelengths of each ray whose corresponding Ewald sphere passes through the zero point $O$ of the reciprocal lattice as well as through the lattice point of the primary reflection $B$ can contribute to the multiple diffraction event, the centres of possible Ewald spheres are the intersection points between the bisector of the reciprocal-lattice vector $\mathbf{h}_{\rm prim}$ (= $OB$ in Fig. 1) and the respective incident ray, *i.e.* the centres have to be located on the horizontal line in Fig. 1(*a*), where the red (blue) sphere corresponds to the minimum (maximum) wavelength with centre $M_{\rm min}$ ($M_{\rm max}$), although all rays between the limiting rays *a* and *b* in Fig. 8(*a*) of Ro-92 comprise the whole range of wavelengths.

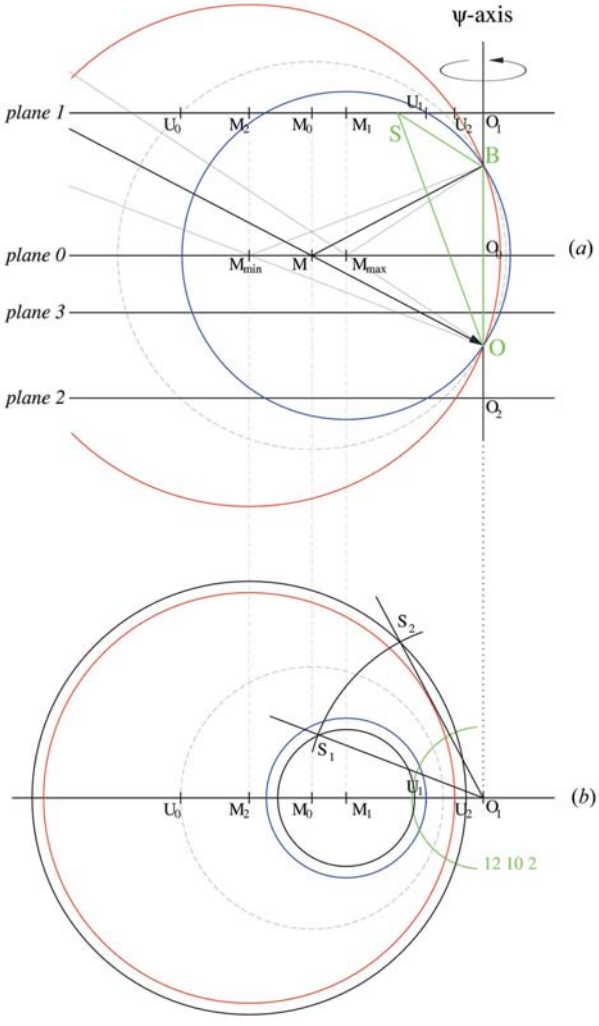


**Figure 1**
The diffraction geometry in reciprocal space with respect to the direction of the $\psi$ axis. (*a*) Elevation. (*b*) Section plane 1.

Keeping in mind that the three vectors $\mathbf{h}_{\rm prim}$, $\mathbf{h}_{\rm op}$ and $\mathbf{h}_{\rm coop}$ form the rigid triangle $OSB$ with side length $d^*_{\rm prim}$, $d^*_{\rm op}$ and $d^*_{\rm coop}$, with $d^*_i = 1/d_i$, where $d_i$ is the appropriate interplanar spacing, the angle between $\mathbf{h}_{\rm prim}$ and $\mathbf{h}_{\rm op}$, $\mu_\psi$, and the components $h_{p,\psi}$ (= $OO_1$ in Fig. 1*a*) and $h_{n,\psi}$ (= $O_1S_1 = O_1S_2$ in Fig. 1*b*) of $\mathbf{h}_{\rm op}$ parallel and normal to $\mathbf{h}_{\rm prim}$ can easily be calculated according to

$$\cos\mu_\psi = (d^{*2}_{\rm prim} + d^{*2}_{\rm op} - d^{*2}_{\rm coop})/(2d^*_{\rm prim}d^*_{\rm op}) \quad (5)$$

$$h_{n,\psi} = d^*_{\rm op}\sin\mu_\psi \quad (6)$$

$$h_{p,\psi} = d^*_{\rm op}\cos\mu_\psi. \quad (7)$$

The profile width in $\psi$ can be deduced from Fig. 1(*b*) representing, as an example, the section plane 1. $M_1U_1$ ($M_2U_2$) is the radius of the blue (red) circle representing the Ewald sphere in this section plane (see Fig. 1*a*). If the broadening by the radius of the perfect spherical crystal sample is taken into consideration, the 'thickness' of the Ewald sphere is additionally broadened by two times $\varepsilon = 1/r$, indicated by the two black circles in Fig. 1(*b*), *i.e.* the reciprocal-lattice 'sphere' with radius $\varepsilon = 1/r$ touches the Ewald sphere first at $S_2$ (reciprocal-lattice point lies outside the Ewald sphere, the distance between the centre of the Ewald sphere and the centre of the reciprocal-lattice 'sphere' is the sum of the radii of the two spheres) and last at $S_1$ (reciprocal-lattice point lies inside the Ewald sphere, the distance between the centre of the Ewald sphere and the centre of the reciprocal-lattice 'sphere' is the difference of the radii of the two spheres). The width of the intensity profile caused by the divergence and wavelength spread of the incident beam and the radius of the crystallite is therefore defined by the angle $\angle(S_1O_1S_2) = \beta_2 - \beta_1$, where $\beta_1$ can be calculated from the triangle $M_1O_1S_1$ and $\beta_2$ from the triangle $M_2O_1S_2$:

$$\begin{aligned}\beta_1 &= a\cos\{(r^2_{11} + h^2_{n,\psi} - r^2_{12})/(2r_{11}h_{n,\psi})\}\\ \beta_2 &= a\cos\{(r^2_{21} + h^2_{n,\psi} - r^2_{22})/(2r_{21}h_{n,\psi})\}\end{aligned} \quad (8)$$

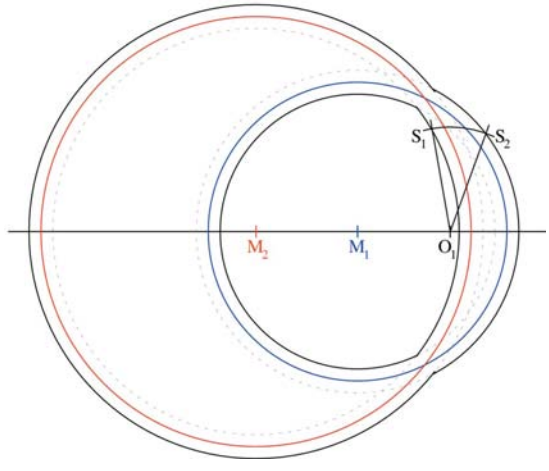


**Figure 2**
The diffraction geometry in reciprocal space with respect to the direction of the $\psi$ axis. Section plane 3 defined in Fig. 1(*a*).

with $r_{11} = M_{\max}O_0 = M_1O_1$, $r_{21} = M_{\min}O_0 = M_2O_1$, $r_{12} = M_1S_1$, $r_{22} = M_2S_2$. It can easily be shown that, with $\lambda^*_{\max} = 1/(\lambda + \Delta\lambda/2)$, $\lambda^*_{\min} = 1/(\lambda - \Delta\lambda/2)$ and $d_1 = O_0O_1$,

$$\begin{aligned} r_{11} &= \{\lambda^{*2}_{\max} - (d^*_{\rm prim}/2)^2\}^{1/2} \\ r_{21} &= \{\lambda^{*2}_{\min} - (d^*_{\rm prim}/2)^2\}^{1/2} \\ r_{12} &= \{(\lambda^*_{\max} - \varepsilon)^2 - d_1^2\}^{1/2} \\ r_{22} &= \{(\lambda^*_{\min} + \varepsilon)^2 - d_1^2\}^{1/2}. \end{aligned} \tag{9}$$

It is obvious from Fig. 1(*a*) that the scheme of the section planes will strongly depend on the distance $d_1$. In Fig. 2, the section plane 3 is shown for comparison. It should be noted that there are two points of intersection between the blue and red Ewald spheres. It can easily be shown that on the right of the two intersection points the expressions for $r_{12}$ and $r_{22}$ have to be replaced by

$$\begin{aligned} r_{12} &= \{(\lambda^*_{\max} + \varepsilon)^2 - d_1^2\}^{1/2} \\ r_{22} &= \{(\lambda^*_{\min} - \varepsilon)^2 - d_1^2\}^{1/2}. \end{aligned} \tag{10}$$

The divergence $\delta_{s,\psi}$ [see expression (4)] which depends on $\theta_{\rm prim}$ can be deduced by means of Ro-92-(Fig. 8*d*). $\delta_{s,\psi}$ is related to $\delta_s$, the divergence of the incident beam in the plane perpendicular to the plane of Fig. 8(*a*) of Ro-92 by

$$\delta_{s,\psi} = 2\arcsin\{\sin(\delta_s/2)/\cos\theta_{\rm prim}\}. \tag{11}$$

$\eta^{\rm op}_\psi$ is the angle of rotation in the plane normal to the $\psi$ axis corresponding to the mosaic spread $\eta$:

$$\eta^{\rm op}_\psi = 2\arcsin\{\sin(\eta/2)/\sin\mu_\psi\}. \tag{12}$$

## 3. Comparison with the experiment

### 3.1. Example for pure *Umweganregung*

The synthetic perfect spherical YIG crystal (radius $r$ = 150 µm) used for the experiment is an example for large absorption and severe primary extinction. The measurement (Fig. 3*b*) was performed on a Enraf–Nonius CAD-4 diffractometer with an Ag tube. The $\psi$-scan pattern of the forbidden 882 reflection is of interest because of the mirror plane at $\psi \sim -24^\circ$ and the extraordinary width of the four peaks at $\psi$ values of about $-56$ and $-47^\circ$ caused by the 12,10,2/$\bar{4}\bar{2}$0 event and of about $-1$ and $8^\circ$ caused by the $\bar{2}\bar{4}$0/10,12,2 event. It is obvious from the corresponding peak location plot (Fig. 3*d*) that the reciprocal-lattice points of the operative reflections corresponding to these *Umweganregung* peaks do not touch the Ag $K\alpha_2$ Ewald sphere. The widths of these peaks therefore mainly arise from the wavelength spread of the Ag $K\alpha_1$ line and the radius of the reciprocal-lattice 'spheres'. The operative reflections 12,10,2 and $\bar{2}\bar{4}$0 pass the Ag $K\alpha_1$ Ewald sphere in the section plane 1 and plane 2 defined in Fig. 1, respectively, both having the same short component $h_{n,\psi}$ (= $O_1S$ = $O_2S$), represented schematically for the 12,10,2 operative reflection by the green arc in Fig. 1*b*.

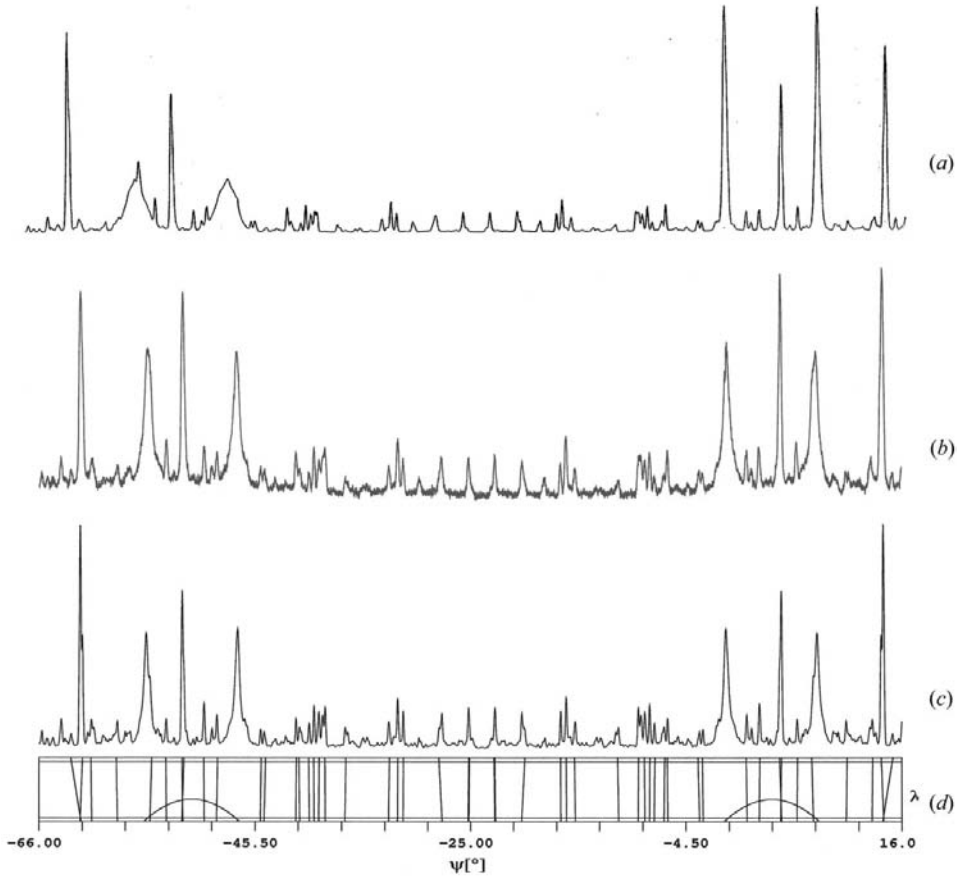


**Figure 3**
The pattern of the 882 reflection of YIG (*a*) calculated with *UMWEG-90*, (*b*) measured with Ag $K\alpha$ radiation, (*c*) calculated with *UMWEG*, (*d*) peak location plot.

In Fig. 3(*a*), the theoretical scan calculated with *UMWEG-90*, *i.e.* using the concept represented in Ro-92-(Fig. 8*a*), is shown (Werner, 1993). As pointed out in §2, this concept predicts a larger peak width for the 12,10,2/$\bar{4}\bar{2}$0 event than for the $\bar{2}\bar{4}$0/10,12,2 event, a prediction which does not agree with the experimental result.

The theoretical scan obtained with *UMWEG* (Ro-99, Ro-03), on the other hand, which is based on Fig. 1, is an excellent simulation of

the experimental pattern. The deviations between the measured and calculated scans in this sample (Figs. 3*b*, *c*) can be attributed to the rough surface of the YIG sample, represented as an electron-microscope image in Rossmanith *et al.* (1993, Fig. 3*b*), *i.e.* to the fact that using the input data of a perfect crystal [Ro-99-(Table 1)] neglects the intensity contribution of the imperfect surface.

### 3.2. Example for multiple diffraction

In Fig. 4, the graphical output of the program *UMWEG* of the multiple diffraction pattern of the very strong $\bar{1}\bar{1}1$ primary reflection of Si (lattice constant $a$ = 5.4282 Å) is shown. The experimental conditions and the sample used for the measurement with synchrotron radiation ($\lambda$ = 1.43765 Å) are identical with those of Ro-00-(§4). The measured upper scan showing three dips is compared with the theoretical lower scan. Because of the fact that the measurement does not show any typical interference effects corresponding to the triplet phases 0 and 180° of the multiple diffraction events [see for example Ro-00-(Fig. 4)], the calculation was performed neglecting the interference term in expression (1). Regarding Table 1 in which the indices, structure factors, intensities, $\psi$ values and FWHMs of the events corresponding to the multiple diffraction pattern of the $\bar{1}\bar{1}1$ primary reflection of Si presented in Fig. 4 are summarized, it becomes clear that the three dips are built up by eight multiple diffraction events, four of them having a very large FWHM (0.7 –0.8°), the other four having the typical FWHM (0.015°) of intensity distributions measured with synchrotron radiation in the 90's at HASYLAB (DESY, Germany). For all events, the *Aufhellung* term is larger than the *Umweganregung* term [expression (1)]. Nevertheless, the agreement between the experimental scan and the theoretical scan calculated according to Ro-06-(5) and Ro-06-(13) is surprisingly good.

**Table 1**
The indices, structure factors, intensities, $\psi$ values and FWHMs of the events corresponding to the multiple diffraction pattern of the $\bar{1}\bar{1}1$ primary reflection of Si presented in Fig. 4.

| $hkl_{op}$ | $F_{op}$ | $hkl_{coop}$ | $F_{coop}$ | $I_{Umw}$ | $I_{Aufh}$ | $\psi$ | FWHM |
|---|---|---|---|---|---|---|---|
| $\bar{3}\bar{1}3$ | 39 | $20\bar{2}$ | 69 | 137 | 397 | 223.360 | 0.804 |
| $\bar{4}04$ | 44 | $3\bar{1}\bar{3}$ | 39 | 31 | 116 | 223.360 | 0.701 |
| $\bar{1}\bar{1}3$ | 45 | $00\bar{2}$ | 0 | 0 | 194 | 224.848 | 0.015 |
| 004 | 58 | $\bar{1}\bar{1}\bar{3}$ | 45 | 22 | 114 | 224.848 | 0.014 |
| $\bar{3}\bar{1}1$ | 45 | 200 | 0 | 0 | 194 | 224.871 | 0.015 |
| $\bar{4}00$ | 58 | $3\bar{1}1$ | 45 | 22 | 114 | 224.871 | 0.014 |
| $\bar{4}04$ | 44 | $3\bar{1}\bar{3}$ | 39 | 31 | 116 | 226.358 | 0.701 |
| $\bar{3}\bar{1}3$ | 39 | $20\bar{2}$ | 69 | 137 | 397 | 226.358 | 0.804 |

## 4. Conclusions

As was shown in §3 and the many examples presented in previous papers of the author, especially in the case of pure *Umweganregung* or pure *Aufhellung*, excellent results can be

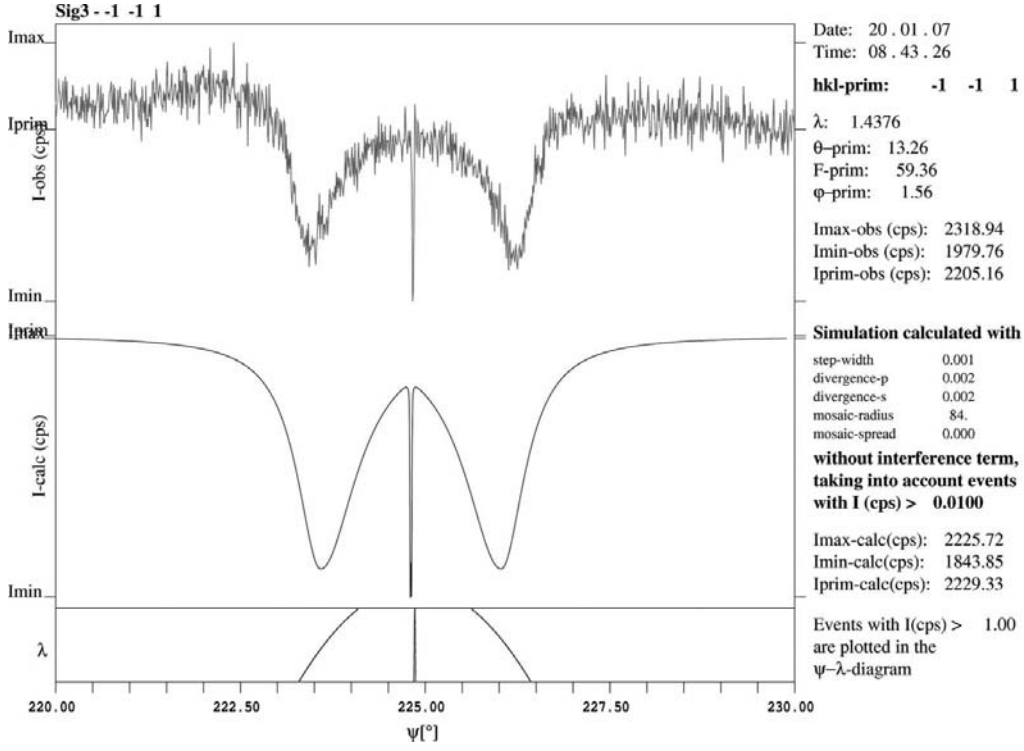


**Figure 4**
Graphical output of *UMWEG* for the $\bar{1}\bar{1}1$ primary reflection of Si measured with synchrotron radiation.

obtained with the program *UMWEG*, which renders the multiple diffraction patterns on an absolute scale.

Reflecting, on the other hand, the many approximations made in the course of derivation of the expressions presented by the author and the large number of variables affecting the height and width of the profiles [modulus and phase of the structure factors involved, Lorentz factors, temperature factors, path lengths, polarization factors, choice of the normalized distribution function, divergence and wavelength spread of the incident beam, shape and mosaicity of the sample, cosine of the angle between the electric vectors of the primary and *Umweg* waves, absorption, primary and secondary extinction and last but not least the approximation Ro-06-(20) for $\varphi_{\rm lattice}(\psi)$], in the framework of the kinematical theory the intensity profile shapes of azimuthal scans of strong primary reflections will scarcely be predictable from the structure factors of the reflections involved (see §4.4 in Weckert & Hümmer, 1997). In most cases, at least qualitative agreement between theory and experiment can be achieved only by taking into account all the above-mentioned variables. Therefore, in the authors opinion, phase determination for *acentric* structures by means of the program *UMWEG* will only be possible in exceptional cases.

In order to enable and simplify further developments and improvements in analysis in the field of kinematical multiple diffraction, the Fortran90 sources of the program *UMWEG* was deposited (IUCr electronic archive, see Ro-07 for details).

## References


Bengel, K. (1991). Diplomarbeit, Universität Hamburg, Germany.
Caticha-Ellis, S. (1975). *Jpn J. Appl. Phys.* **14**, 603–611.
Chang, S.-L. & Post, B. (1975). *Acta Cryst.* A**31**, 832–835.
Collela, R. & Merlini, A. (1966). *Phys. Status Solidi*, **18**, 157–167.
Cousins, C. S. G., Gerward, L. & Staun-Olsen, J. (1978). *Phys. Status Solidi*, **48**, 113–119.
Laue, M. von (1960). *Röntgenstrahlinterferenzen.* Frankfurt am Main: Akademische Verlagsgesellschaft.
Mathieson, A. McL. (1994). *Acta Cryst.* A**50**, 123–126.
Moon, R. M. & Shull, C. G. (1964). *Acta Cryst.* **17**, 805–812.
Post, B. (1975). *J. Appl. Cryst.* **8**, 452–456.
Post, B. (1976). *Acta Cryst.* A**32**, 292–296.
Prager, P. R. (1971). *Acta Cryst.* A**27**, 563–569.
Renninger, M. (1937). *Z. Phys.* **106**, 141–176.
Rossmanith, E. (1992). *Acta Cryst.* A**48**, 596–610.
Rossmanith, E. (1993). *Acta Cryst.* A**49**, 80–91.
Rossmanith, E. (1999). *J. Appl. Cryst.* **32** 355–361.
Rossmanith, E. (2000). *J. Appl. Cryst*. **33**, 921–927.
Rossmanith, E. (2002*a*). *Acta Cryst.* A**58**, 12–20.
Rossmanith, E. (2002*b*). *Acta Cryst.* A**58**, 473–486.
Rossmanith, E. (2003). *J. Appl. Cryst.* **36**, 1467–1474.
Rossmanith, E. (2004). *J. Appl. Cryst.* **37**, 493–497.
Rossmanith, E. (2006). *Acta Cryst.* A**62**, 174–177.
Rossmanith, E. (2007). *J. Appl. Cryst.* **40**, 185–187.
Rossmanith, E., Adiwidjaja, G., Eck, J., Kumpat, G. & Ulrich, G. (1994). *J. Appl. Cryst.* **27**, 510–516.
Rossmanith, E. & Bengel, K. (1995). *Acta Cryst.* A**51**, 134–142.
Rossmanith, E., Werner, M., Kumpat, G. & Ulrich, G. (1993). *J. Appl. Cryst.* **26**, 756–762.
Unangst, D. & Melle, W. (1975). *Acta Cryst.* A**31**, 234–235.
Weckert, E. & Hümmer, K. (1997). *Acta Cryst.* A**53**, 108–143.
Werner, M. (1993). Diplomarbeit, Universität Hamburg, Germany.